Gallacher, K., Millar, R.W., Ballabio, A., Frigerio, J., Bashir, A., MacLaren, I., Isella, G., Ortolani, M., and Paul, D.J. (2016) Mid-Infrared Intersubband Absorption from P-Ge Quantum Wells on Si. In: 41st International Conference on Infrared, Millimeter, and Terahertz Waves (IRMMW-THz 2016), Copenhagen, Denmark, 25-30 Sept 2016, ISBN 9781467384858 (doi:10.1109/IRMMW-THz.2016.7758421)

Mid-infrared intersubband absorption from p-Ge quantum wells on Si

K. Gallacher,[1] R. W. Millar,[1] A. Ballabio,[2] J. Frigerio,[2] A. Bashir,[3] I. MacLaren,[3] G. Isella,[2]
M. Ortolani,[4] and D.J. Paul[1]

[1] University of Glasgow, School of Engineering, Rankine Building, Glasgow, G12 8LT, U.K.
[2]L-NESS, Dipartimento di Fisica del Politecnico di Milano, Como, 22100 Italy
[3]University of Glasgow, School of Physics and Astronomy, Kelvin Building , Glasgow G12 8QQ, U.K.
[4]Center for Life Nanosciences, Istituto Italiano di Tecnologia, Rome, 00185 Italy

Abstract— **Mid-infrared intersubband absorption from p-Ge quantum wells with $Si_{0.5}Ge_{0.5}$ barriers grown on a Si substrate is demonstrated from 6 to 9 µm wavelength at room temperature and can be tuned by adjusting the quantum well thickness. Fourier transform infra-red spectroscopy measurements demonstrate clear absorption peaks corresponding to intersubband transitions among confined hole states. The work indicates an approach that will allow quantum well intersubband photodetectors to be realized on Si substrates in the important atmospheric transmission window of 8-13 µm.**

I. INTRODUCTION

There is an increased interest to develop Si based detectors that cover the important transmission windows within the mid-infrared (3-5 and 8-13 µm). Applications that could take advantage of this cheaper platform are biological and gas sensing spectroscopy [1-3]. SiGe quantum well (QW) infrared photodetectors have been previously demonstrated. However, these devices are limited to low detectivities due to the relatively large electron and hole effective masses and critical thickness limitations imposed by growth. Recently, intersubband absorption from p-Ge QWs has been experimentally demonstrated for the first time [2]. Ge QWs have the potential to improve performance significantly due to the lower effective masses and by allowing strain symmetrisation of the growth.

II. RESULTS

Here we demonstrate strain symmetrized growth of 500 periods of Ge QWs with $Si_{0.5}Ge_{0.5}$ barriers on $Si_{0.2}Ge_{0.8}$ virtual substrates grown on top of (001) Si. The band energies and confined wave-functions were calculated using a self-consistent 8-band k.p Poisson-Schrödinger solver with periodic boundary conditions orientated along the growth-axis and the deformation potentials from ref [3]. Fig. 1 presents the calculated band structure for an 8.1 nm Ge QW and 5.2 nm $Si_{0.5}Ge_{0.5}$ barriers on a relaxed $Si_{0.2}Ge_{0.8}$ buffer. The ground state in the QW is HH1 due to strain splitting of the HH and LH bands. The HH2 and HH3 are at roughly the same energy as the LH1 and LH2 subband states, respectively. For a doping level of $N_A \approx 10^{18}$ cm^{-3} within the QW, the Fermi level at 300 K resides at the HH2 band. Therefore, the HH2-HH3 intersubband transition should be optically active. The samples were grown by low energy plasma enhanced chemical vapour deposition on a high resistivity Si substrate [4]. A 500 nm thick $Si_{0.6}Ge_{0.4}$ layer was first grown followed by a 500 nm linear graded buffer. Then an undoped 10 nm $Si_{0.2}Ge_{0.8}$ spacer region was grown followed by the active region consisting of 500 periods of compressively strained Ge QWs (tensile strained $Si_{0.5}Ge_{0.5}$ barriers) of 8.1 (5.4) nm thickness. Lastly, another undoped 10 nm $Si_{0.2}Ge_{0.8}$ spacer layer was grown, followed by a 20 nm $Si_{0.2}Ge_{0.8}$ cap region.

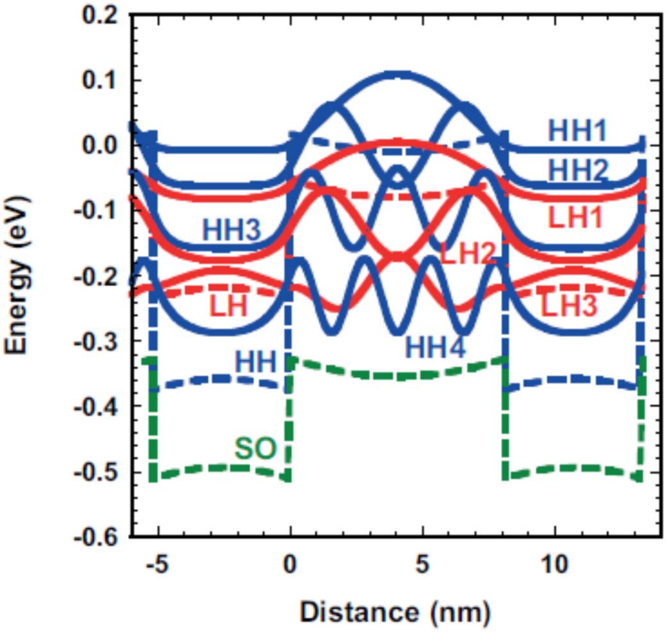

Fig. 1. A schematic diagram of the calculated band structure for an 8.1 nm Ge quantum well sandwiched between 5.2 nm $Si_{0.5}Ge_{0.5}$ barriers. The squared wave-functions for the lowest energy subband states for the heavy hole (HH) and light hole (LH) bands are shown.

Heterolayer thicknesses of the grown superlattice structure were measured by scanning transmission electron microscopy (STEM). The STEM was performed on a probe-corrected JEOL ARM 200F equipped with a cold field emission gun operated at 200 kV. A Gatan GIF Quantum ER energy filter/ spectrometer equipped with a fast dual electron energy loss spectroscopy (EELS) system was used. The STEM was operated in high angle annular dark field mode (HAADF). Atomic contrast image was obtained by the detection of elastically and quasi-elastically scattered electrons using a HAADF. Therefore, this is a well-suited method for imaging Ge and SiGe interfaces. The HADDF STEM image in Fig. 2 (a) demonstrates the smooth and abrupt interfaces between the Ge QWs and the $Si_{0.5}Ge_{0.5}$ barriers for the 8.1 nm QW superlattice structure. Fig. 2 (b) is the calculated QW (barrier) thickness as measured from STEM analysis. There is a slight variation of the QW and barrier thicknesses throughout the superlattice growth.

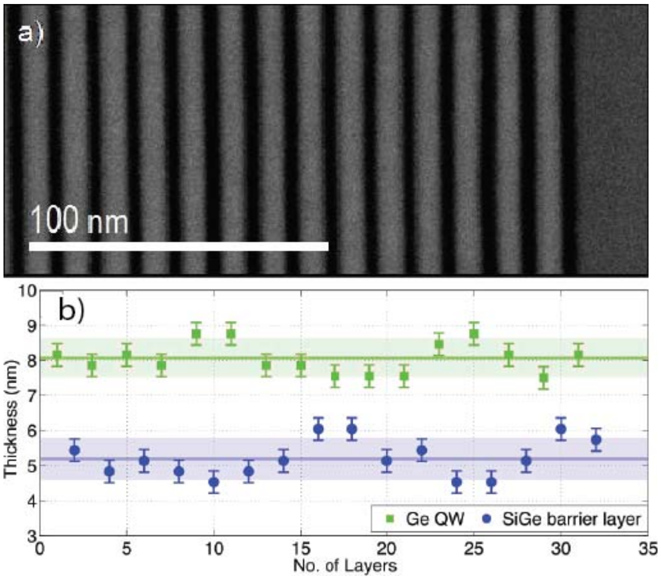

Fig. 2. (a) A scanning transmission electron microscope (STEM) image of the 8.1 nm Ge quantum well structure by high angle annular dark field mode. Due to the Z^2 dependence, heavier atoms appear brighter because of strong scattering at high angles while lighter atoms appear darker. Therefore, lighter regions in this image correspond to Ge QWs and the darker regions correspond to the SiGe barriers. (b) The thickness variation of the superlattice structure as obtained from STEM analysis. In this case the Ge QWs have an average thickness of ~ 8.1 nm (green line) and the SiGe barriers are ~ 5.2 nm thick (blue line).

Fourier transform infrared (FTIR) transmission measurements were performed on the as-grown 8.1 nm QW structure in vacuum at temperatures ranging from 6 to 300 K. The setup consisted of a Bruker IFS 66v interferometer and a nitrogen-cooled MCT detector. Blank chips were bonded onto the cold finger of an optical cryostat aligned within the sample chamber of the FTIR. Measurements were performed in surface normal (x-y) geometry with in-plane (TE) light polarization state defined by the properties of the Michelson interferometer. The electric field component parallel to the growth axis (TM) was null at all wavelengths before hitting the sample, but due to the refractive index variation of the complete structure and the backside of the substrate being unpolished, there will be some scattering that couples some of the radiation into TM polarized active transitions, so both TE and TM transitions will be observed. Fig. 3 (a) demonstrates the 300 K FTIR absorption spectra for the 8.1 nm QW structure. The absorption peak at ~ 170 meV corresponds to a bound-to-continuum transition within the QW. The relatively narrow peak at ~ 140 meV corresponds to vibrational interstitial oxygen impurities from the Si substrate. The modelled intersubband absorption is also shown for a TE (xy) and TM (z) polarization. The model agrees reasonably well with the experimental peak positions but at present underestimates the absorption width due the modelling not being able to account for broadening effects such as inhomogeneous broadening. Fig. 3 (b) demonstrates the low temperature FTIR absorption spectra for the 8.1 nm QW. In this instance the absorption peak from the Si-O interstitial defect can be used as a temperature reference since it blue shifts with decreasing temperature and begins to exhibit a narrow line-width below 10 K, which is evident in the 6 K spectra. It is clear that as the temperature is decreasing the intersubband absorption increases. There is a negligible intersubband absorption temperature dependence observed. This arises from how both the band-edges of the barriers and QWs are changing at approximately the same rate in energy and produce a negligible change in terms of the QW depth for both the HH and LH bands. It is also evident from the spectra that there is a longer wavelength absorption peak appearing with decreasing temperature at ~ 116 meV. Most likely, the Fermi level enters the HH1 subband at low temperature, activating the HH1-HH2 transition. Doping-dependent analysis will be needed to address this point further.

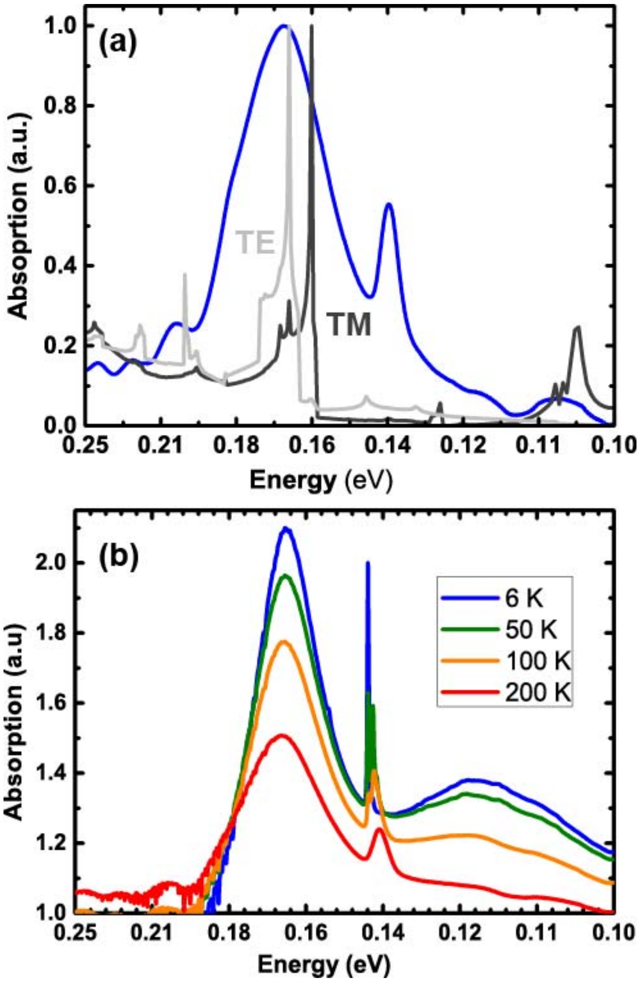

Fig. 3. (a) Fourier transform infra-red (FTIR) absorption spectra at 300 K under vacuum for the as-grown 8.1 nm Ge quantum well (QW) structure. The modelled intersubband absorption spectra for TM and TE polarization as calculated from NextNano simulations is also displayed. (b) The low temperature FTIR absorption spectra of the 8.1 nm QW structure from 6-200 K.

REFERENCES

[1] Baldassarre L., *et al.* “Mid-infrared plasmon-enhanced with germanium antennas on silicon substrates”; Nano Letters; **15** ,7225 (2015).

[2] Millar, R., et al., Extending the emission wavelength of Ge nanopillars to 2.25 µm using silicon nitride stressors. Optics express, 2015.

[3] Millar, R., et al., Analysis of Ge micro-cavities with in-plane tensile strains above 2%. Optics Express, 2016.

[4] Gallacher, K., et al., Mid-infrared intersubband absorption from p-Ge quantum wells grown on Si substrates. Applied Physics Letters, 2016.

[5] Paul, D.J., 8-band k.p modeling of the quantum confined Stark effect in Ge quantum wells on Si substrates. Physical Review B, 2008.

[6] Isella, G., et al., Low-energy plasma-enhanced chemical vapor deposition for strained Si and Ge heterostructures and devices. Solid-State Electronics, 2004.